JOURNAL OF GEOPHYSICAL RESEARCH, VOL. 105, NO. D8, PAGES 9971–9979, APRIL 27, 2000

Case studies of the vertical structure of the direct shortwave aerosol radiative forcing during TARFOX

J. Redemann,[1] R.P. Turco,[2] K.N. Liou,[2] P.V. Hobbs,[3] W.S. Hartley,[3] R.W. Bergstrom,[1] E.V. Browell,[4] and P.B. Russell[5]

Abstract. The vertical structure of aerosol-induced radiative flux changes in the Earth's troposphere affects local heating rates and thereby convective processes, the formation and lifetime of clouds, and hence the distribution of chemical constituents. We present observationally based estimates of the vertical structure of direct shortwave aerosol radiative forcing for two case studies from the Tropospheric Aerosol Radiative Forcing Observational Experiment (TARFOX) which took place on the U.S. east coast in July 1996. The aerosol radiative forcings are computed using the Fu-Liou broadband radiative transfer model. The aerosol optical properties used in the radiative transfer simulations are calculated from independent vertically resolved estimates of the complex aerosol indices of refraction in two to three distinct vertical layers, using profiles of *in situ* particle size distributions measured aboard the University of Washington research aircraft. Aerosol single-scattering albedos at 450 nm thus determined range from 0.9 to 0.985, while the asymmetry factor varies from 0.6 to 0.8. The instantaneous shortwave aerosol radiative forcings derived from the optical properties of the aerosols are of the order of -36 W m^{-2} at the top of the atmosphere and about -56 W m^{-2} at the surface for both case studies.

1. Introduction

Current interest in atmospheric aerosols derives in part from the assessments of the Intergovernmental Panel on Climate Change (IPCC) regarding the potential importance of radiative forcing of climate by tropospheric aerosols [*IPCC*, 1995]. For the purpose of this paper, "radiative forcing" due to a radiatively active species is defined as the change in net radiative flux (shortwave plus longwave) at a given level in the atmosphere due to the presence of this species in the Earth-atmosphere system. The total aerosol radiative forcing can be broken down into the direct effect due to the actual interaction of the aerosols with radiation and the indirect effect due to aerosol-induced changes in the radiative properties of clouds. The IPCC estimates of the globally averaged direct and indirect aerosol radiative forcings due to changes in atmospheric composition over the last few decades are both on the order of -1 W m^{-2}, with larger uncertainties in the estimates of the indirect effect. If, in fact, the total anomalous aerosol forcing amounts to -2 W m^{-2}, it attains a magnitude comparable to the positive radiative forcing anomaly attributed to the greenhouse gases, CO_2, N_2O, and CH_4. However, the IPCC 1995 assigns a low confidence to the estimate of the direct aerosol effect and a very low confidence to the estimate of the indirect effect. In reality, there is very little scientific basis for making such estimates, especially given the uncertainty in the radiative forcing associated with background aerosols and their natural variations.

The low confidence in the estimates of aerosol radiative perturbations is caused by the highly nonuniform compositional, spatial, and temporal distributions of tropospheric aerosols on a global scale owing to their heterogeneous sources and short lifetimes. Nevertheless, recent studies have shown that the inclusion of aerosol effects in climate model calculations can improve agreement with observed spatial and temporal temperature distributions [*Hansen et al.*, 1995; *Tett et al.*, 1996; *Haywood and Ramaswamy*, 1998]. Accordingly, it is crucial to establish a sound observational basis for estimating the magnitude of the absolute, and perturbed, global aerosol forcing, as well as its geographical distribution.

Hansen et al. [1997] studied the sensitivity of climate to the vertical distribution of a globally uniform "ghost" forcing of 4 W m^{-2} (for example, due to aerosols). They found that global surface temperature changes associated with this forcing are quite sensitive to the altitude at which the forcing occurs. Hence it is important to devise techniques that cannot only determine a column-averaged aerosol radiative forcing but methods that provide estimates of the vertically resolved radiative forcing.

In this paper we present vertically resolved estimates of the direct shortwave aerosol radiative forcing based on (1) the determination of the effective aerosol complex index of refraction in distinct horizontal layers obtained from a combination of lidar-derived aerosol backscatter, sunphotometer-derived aerosol optical depths and *in situ* particle size distribution measurements [*Redemann et al.*, this issue]; (2) vertical profiles of aerosol particle size distributions measured aboard the University of Washington research aircraft [*Hobbs*, 1999]; (3) vertical profiles of lidar-derived water vapor obtained form the LASE (Lidar Atmospheric Sensing Experiment) instrument [*Ferrare et al.*, this

[1] Bay Area Environmental Research Institute, San Francisco, California.
[2] Department of Atmospheric Sciences, University of California, Los Angeles.
[3] Department of Atmospheric Sciences, University of Washington, Seattle.
[4] NASA Langley Research Center, Hampton, Virginia.
[5] NASA Ames Research Center, Moffett Field, California.

Paper number 1999JD901042.
0148-0227/00/1999JD901042$09.00

issue; *Browell et al.*, 1996]; and (4) radiative flux simulations with the Fu-Liou radiative transfer model [*Fu and Liou*, 1992, 1993].

2. Data Sources

One of the main goals of the Tropospheric Aerosol Radiative Forcing Observational Experiment (TARFOX) is to reduce uncertainties in estimates of tropospheric aerosol radiative forcing of climate [*Russell et al.*, 1999a]. To calculate solar radiative fluxes with the Fu-Liou radiative transfer model, a quantification of the amounts of radiatively active gases and the aerosol single-scattering parameters including the extinction coefficient, asymmetry factor, and single-scattering albedo is necessary. For the determination of aerosol scattering parameters the following approach was used. Estimates of the aerosol refractive indices at 815 nm derived by *Redemann et al.* [this issue] were utilized for the first two bands of the Fu-Liou radiative transfer model (0.2 - 1.3 μm). These estimates are obtained by comparing vertically resolved *in situ* particle size distribution measurements ($0.05 < r < \sim 11.8$ μm) with lidar-derived aerosol backscatter and sunphotometer-derived aerosol optical depths and by determining which aerosol complex index of refraction best reproduces the remote sensing measurements when assumed in a Mie calculation based on the particle size distribution measurements in a given vertical layer of the atmosphere. The results of the study by *Redemann et al.* [this issue] are particle size distribution measurements and estimates of the effective aerosol refractive indices in distinct vertical layers which result in closure with the lidar-derived aerosol backscatter and the sunphotometer-derived aerosol optical depth, respectively.

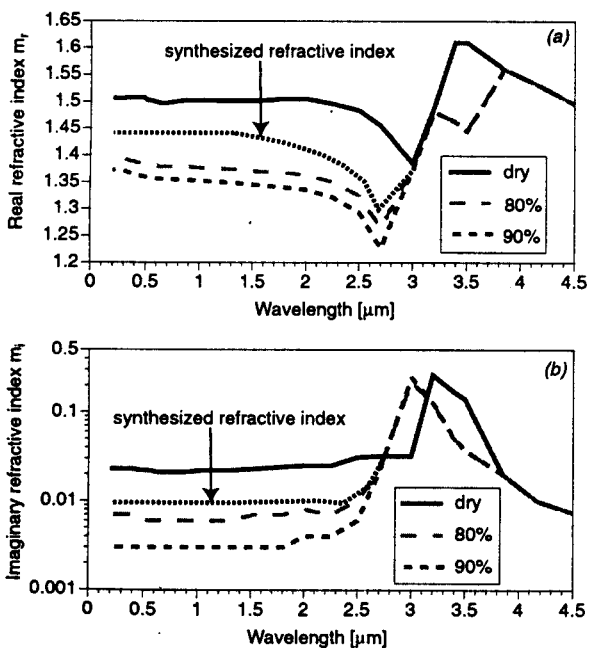

Figure 1. Example of synthesis of the complex aerosol index of refraction for input into the Fu-Liou radiative transfer model. The 80% relative humidity TARFOX average aerosol refractive index from the ELSIE model is used to extrapolate the refractive indices estimated by *Redemann et al.* [this issue].

Redemann et al. [this issue] also validated the assumption that the aerosol refractive index is constant in the sunphotometer wavelength range (0.38 - 1.02 μm). For wavelengths beyond 1.3 μm the aerosol refractive indices, modeled by P. Hignett (private communication), were incorporated. These refractive indices are obtained using the ELSIE model [*Lowenthal et al.*, 1995] based on average TARFOX aerosol chemical composition measurements by *Novakov et al.* [1997] and *Hegg et al.* [1997].

Figure 1 shows the ELSIE-derived average TARFOX aerosol complex index of refraction for three relative humidities of 0%, 80% and 90%. It is noteworthy that there is no difference in the refractive indices at 80% and 90% RH for wavelengths greater than about 2.9 μm. Therefore for wavelengths greater than 2.9 μm the 80% RH TARFOX average refractive were used in this study. For wavelengths between 1.3 and 2.9 μm the refractive indices were calculated by gradually decreasing the difference between the refractive index derived by *Redemann et al.* [this issue] and the 80% RH TARFOX refractive index at 1.3 μm as a function of wavelength, so the difference vanishes at a wavelength of 2.9 μm.

This process was used for both the real and the imaginary parts of the aerosol complex index of refraction. It is schematically illustrated in Figure 1 for a hypothetical case study in which the technique by *Redemann et al.* [this issue] obtained a best fit backscatter aerosol refractive index of 1.44 - 0.01i at 815 nm. The resulting curve (dotted lines in Figure 1, labeled "synthesized refractive index") is constant in the region 0.2 μm < λ < 1.3 μm, asymptotically approaches the 80% RH refractive index in the region between 1.3 and 2.9 μm, and is identical with the 80% RH refractive index for wavelengths greater than 2.9 μm. In this way, the TARFOX-average compositional analysis supplied the aerosol index of refraction in the part of the spectrum where no optical measurements were available to help constrain the choice of the aerosol refractive index.

Based on the wavelength-dependent aerosol refractive indices in distinct horizontal layers, and the profiles of *in situ* particle size distributions measured aboard the UW C-131A aircraft, the vertical profiles of aerosol single-scattering properties (i.e., the aerosol extinction coefficient, single-scattering albedo, and asymmetry factor) can be calculated as a function of altitude.

Since the 18 bands in the Fu-Liou radiative transfer model are relatively broad, the aerosol radiative properties for a given band and altitude were obtained by integrating over the band width. For instance, the average aerosol single-scattering albedo $\bar{\omega}$ in the first band (0.2 μm < λ < 0.7 μm) can be obtained from

$$\bar{\omega} = \int_{0.2}^{0.7} \omega(\lambda) d\lambda \Big/ \int_{0.2}^{0.7} d\lambda. \quad (1)$$

Similarly, the aerosol extinction coefficient and asymmetry factor can be calculated. After the aerosol optical properties for the 18 bands of the Fu-Liou model have been calculated as a function of altitude, we can obtain the direct shortwave aerosol radiative forcing by subtracting the net irradiances (downward minus upward) in the radiative transfer model runs with aerosols from those without aerosols as follows:

$$\Delta_a F(z) = F_a(z) - F_{na}(z). \quad (2)$$

In this study we present only computations of the shortwave aerosol forcing, covering the first six bands of the Fu-Liou model (0.2 to 4.0 μm). This choice is based on the fact that the estimates of aerosol refractive indices by *Redemann et al.* [this issue] are obtained from measurements of aerosol optical properties in the

Table 1. Summary of Data Sources From TARFOX Used for Aerosol Radiative Forcing Calculations Described in This Paper

Quantity	Source of Data	Vertical Resolution
Aerosol size distributions	measured *in situ* aboard the UW C-131A aircraft using three aerosol spectrometers	~100 m
Complex aerosol refractive indices	0.2 μm < λ < 1.3 μm - determined by refractive index retrieval method developed by *Redemann et al.* [this issue]; 1.3 μm < λ < 2.9 μm - see above, but asymptotically approaching the TARFOX-average 80% RH refractive indices from the ELSIE model; 2.9 μm < λ < 4.0 μm - TARFOX-average 80% RH	two or three distinct vertical layers, as indicated by the refractive index retrieval method of *Redemann et al.* [this issue]
Aerosol single-scattering properties	*in situ* particle size distribution measurements and estimated effective aerosol refractive indices (see above)	same as size distribution measurements, ~100 m
Water vapor profiles	derived from LASE differential absorption lidar (DIAL) measurements	30 m (in part of profile with sufficient H_2O)
Ozone profiles	midlatitude summer standard atmosphere data	60-70 layers between 0.1 hPa and surface
p, T	measured *in situ* aboard the UW C-131A, taken from nearby radiosondes above aircraft	100 m (UW C-131A)
Surface albedo	parameterization by *Taylor et al.* [1996] and *Glew et al.* [1998] as function of solar zenith angle	NA

visible to near-infrared part of the spectrum, where most of the solar energy resides. Therefore an extrapolation of these refractive indices into the IR part of the spectrum cannot be justified and should only be performed when additional optical measurements in that part of the spectrum are available. Moreover, because of their sizes, aerosols are usually considered to be more important for their influence on solar radiation.

The most important gaseous atmospheric constituent affecting the aerosol radiative forcing is water vapor, since it potentially alters the amount of solar flux incident on the aerosol layers. For the TARFOX radiative flux calculations the profiles of water vapor were provided by the LASE differential absorption lidar (DIAL) system aboard the ER-2 aircraft. This system has been intercompared with *in situ* sensors and has been shown to measure water vapor concentrations across the entire troposphere to an accuracy of better than 6% or 0.01 g/kg, whichever is greater [*Browell et al*, 1996; *Ferrare et al.*, this issue].

Ozone profiles for the radiative transfer calculations were taken from midlatitude summer standard atmosphere data, while the CO_2 mixing ratio was fixed at 350 ppm. Profiles of pressure and temperature were measured *in situ* aboard the UW C-131A aircraft. For altitudes above the aircraft ceiling, data from balloon sondes launched from Wallops Island, Virginia, during TARFOX were utilized.

Aerosol-induced radiative flux changes are a strong function of the solar zenith angle and the albedo of the underlying surface. Estimates of the ocean surface albedo A_S were taken from a parameterization developed by *Taylor et al.* [1996] and *Glew et al.* [1998] who used a large set of over-ocean measurements to derive the following expression for the wavelength-independent surface albedo [*Briegleb and Ramanathan*, 1982]:

$$A_S = \frac{0.037}{1.1\mu_o^{1.4} + 0.15}, \quad (3)$$

where μ_o is the cosine of the solar zenith angle. Table 1 summarizes the data sources for the radiative flux calculations in this work.

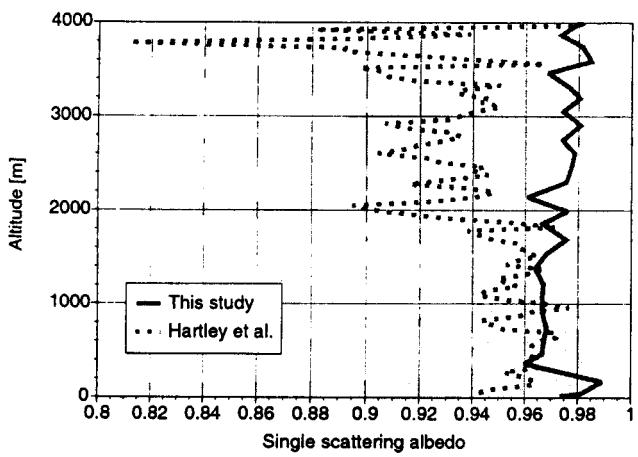

Figure 2. Single-scattering albedo (solid line) for the first band of the Fu-Liou radiative transfer model (0.2 μm < λ < 0.7 μm) for TARFOX case study 1, July 17, 1996, derived using *in situ* particle size distributions and effective aerosol refractive index estimates from *Redemann et al.* [this issue]. For comparison, independently measured single-scattering albedos at 450 nm from *Hartley et al.* [this issue] are shown (dotted line). The gray shaded area represents their error estimates based on one standard deviation plus instrumental error.

3. Radiative Transfer Simulations

3.1. Radiative Flux Calculations for July 17, 1996

For this case study, equation (1) (and its analogs for extinction coefficient and asymmetry factor) yields the vertical profile of the single-scattering albedo shown in Figure 2 and extinction and asymmetry factor in Figure 3 (for the first band of the Fu-Liou model). The aerosol refractive indices obtained from the retrieval technique developed by *Redemann et al.* [this issue] were 1.33 - 0.00117*i* for the surface layer (0-250 m), 1.378 - 0.00428*i* for the layer between 250 and 1650 m, and 1.451 - 0.00224*i* for the layer extending from 1650 to 4030 m. A number of

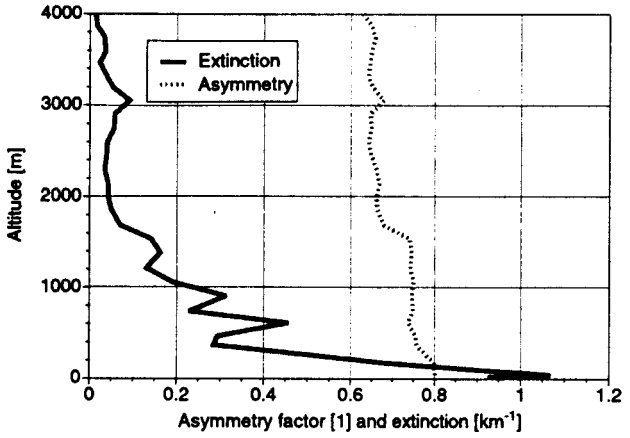

Figure 3. Aerosol extinction coefficient and asymmetry factor for the first band of the Fu-Liou radiative transfer model (0.2 μm < λ < 0.7 μm) for TARFOX case study 1, July 17, 1996.

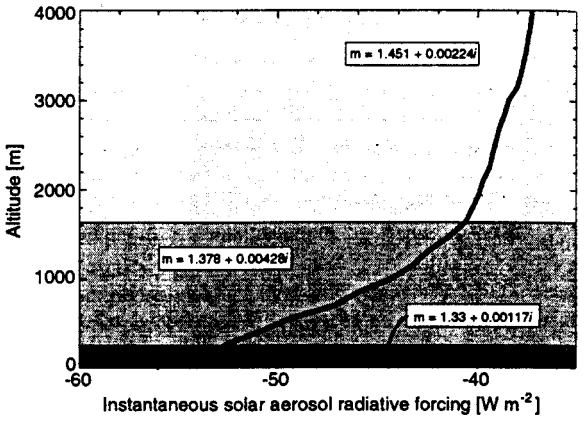

Figure 4. Vertical profile of the instantaneous shortwave aerosol radiative forcing, as calculated by the Fu-Liou radiative transfer model for TARFOX case study 1, July 17, 1996, 1430 GLT for a surface albedo A_S of 3.8% and μ_0 of 0.81. The forcing at the top of the atmosphere (TOA) is -35.91 W m^{-2}.

investigators [e.g., *Ackerman and Toon,* 1981; *Bohren and Huffman*, 1983] have pointed out that an effective refractive index as derived from an optical scattering measurement may lead to erroneous estimates of the aerosol absorption coefficient and thereby the single-scattering albedo. To validate our single-scattering albedo profiles, Figure 2 shows a comparison of our data to values derived from *in situ* measurements of aerosol extinction and absorption using nephelometers and aerosol soot absorption photometers, respectively [*Hartley et al.*, this issue]. The gray shaded area in Figure 2 represents error estimates by *Hartley et al.* [this issue], comprised of one standard deviation plus instrumental errors. In general, the two entirely different methods show good agreement within the error bars and yield very good agreement for the data below 2000 m where most of the aerosol optical depth occurs. The single-scattering albedo is lowest for the middle layer with a value of about 0.96 and shows values between 0.97 and 0.985 for the other two layers.

The asymmetry factor (shown in Figure 3), on the other hand, is largest for the surface layer, where the *in-situ*-measured particle size distributions contained large particles.

For the time and location of this case study, the parameterization of the surface albedo by *Glew et al.* [1998] (compare equation (3)) yields a value of 3.8% for μ_0 = 0.81. Figure 4 shows the results for the vertical profile of the instantaneous shortwave aerosol radiative forcing. The top of the atmosphere (TOA) aerosol radiative forcing calculations for this case yield a value of -36 W m^{-2}, while the forcing at the surface is -56 W m^{-2}. Most of the forcing occurs in the aerosol layer between 250 and 1650 m, which accounts for most of the aerosol optical depth (midvisible optical depth of ~0.35). However, the relatively shallow surface layer beneath 250 m also contributes significantly.

Since the aerosol radiative forcing is a strong function of the solar zenith angle and the surface albedo, the diurnal variation of the aerosol radiative forcing needs to be estimated in order to compare the instantaneous forcing values at a certain time of the day to other case studies under different conditions. However, there is no information on the temporal evolution of the aerosol layers detected in case study 1. Accordingly, a time dependence of the forcing results presented here can only be introduced by varying the solar zenith angle and the surface albedo. The diurnal dependence of the shortwave aerosol radiative forcing resulting from this variation is shown in Figure 5.

Figure 5 shows the distinct noontime minimum of the aerosol radiative forcing and maxima in the midmorning and midafternoon, which have been reported previously [e.g., *Russell et al.*, 1999b]. Since the case study on this day took place at ~1430 Genuine Local Time (GLT) (870 min), Figure 5 shows that a value of approximately -36 W m^{-2} for the TOA radiative forcing is representative for the forcing throughout this day in that it is a fairly good average value between the noontime minimum of about -31 W m^{-2} and the afternoon maximum of some -43 W m^{-2}.

3.2. Radiative Flux Calculations for July 24, 1996

Figures 6 and 7 show the derived aerosol optical parameters in the first band of the Fu-Liou radiative transfer model for the July

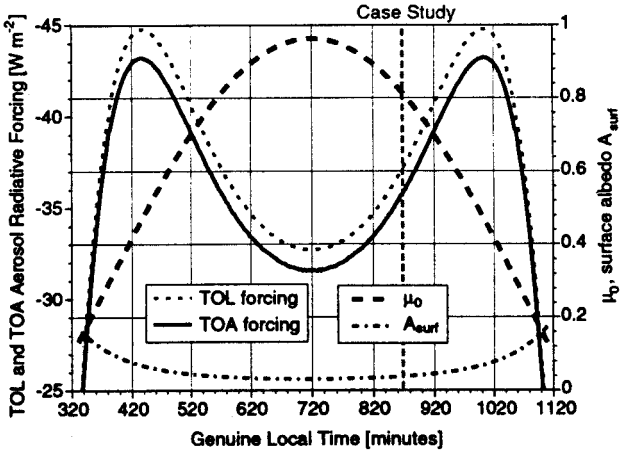

Figure 5. Estimate of the diurnal variation of the instantaneous shortwave aerosol radiative forcing, as calculated by the Fu-Liou radiative transfer model for TARFOX case study 1, July 17, 1996, for the top of the atmosphere (TOA, solid line) and the top of the aerosol layer (TOL, short-dashed line) by varying only the solar zenith angle and the ocean surface albedo with time. The diurnal variation of ocean surface albedo and μ_0 are indicated.

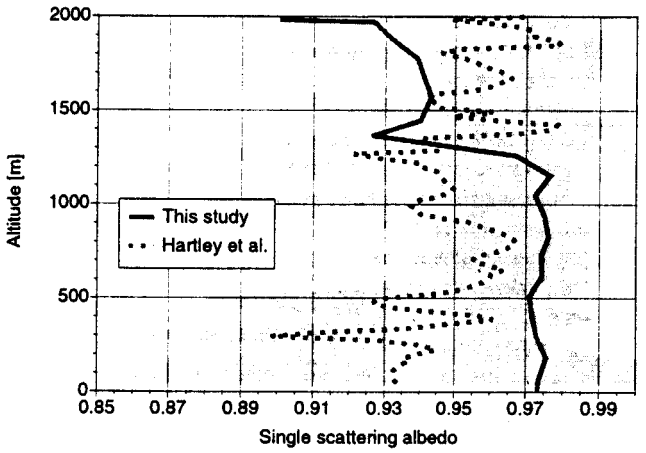

Figure 6. Single-scattering albedo (solid line) for the first band of the Fu-Liou radiative transfer model (0.2 μm < λ < 0.7 μm) for TARFOX case study 2, July 24, 1996, derived using *in situ* particle size distributions and effective aerosol refractive index estimates from *Redemann et al.* [this issue]. For comparison, independently measured single-scattering albedos at 450 nm from *Hartley et al.* [this issue] are shown (dotted line). The gray shaded area represents their error estimates based on one standard deviation plus instrumental error.

24, 1996, case study at 1500 GLT (900 min). The aerosol refractive indices for this case study were estimated to be 1.451 - 0.00345*i* for the lower layer (150 to 1280 m) and 1.451 - 0.00819*i* for the layer extending from 1280 to 1980 m [*Redemann et al.*, this issue]. The single-scattering albedo in Figure 6 clearly shows the aerosol layer structure, with values ranging from approximately 0.975 in the lower layer to values between 0.90 and 0.94 in the layer above 1280 m. These values are again in good agreement with independently determined single-scattering albedos by *Hartley et al.* [this issue] (see Figure 6).

Aerosol refractive indices retrieved for the layer above 150 m were used for the calculations of the optical properties of the two aerosol size distributions below 150 m. The aerosol asymmetry factor and extinction thus determined are shown in Figure 7.

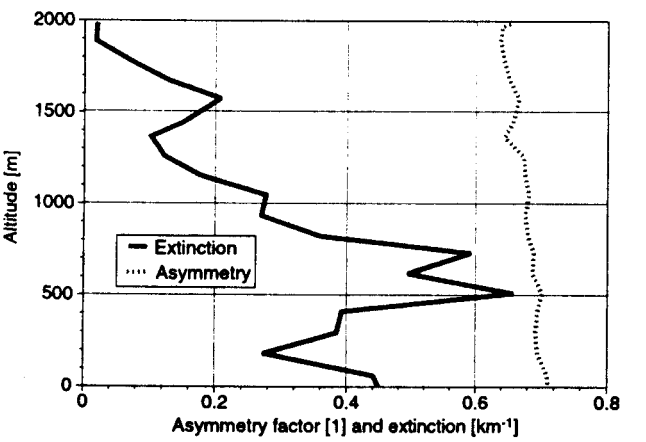

Figure 7. Aerosol extinction coefficient and asymmetry factor for the first band of the Fu-Liou radiative transfer model (0.2 μm < λ < 0.7 μm) for TARFOX case study 2, July 24, 1996.

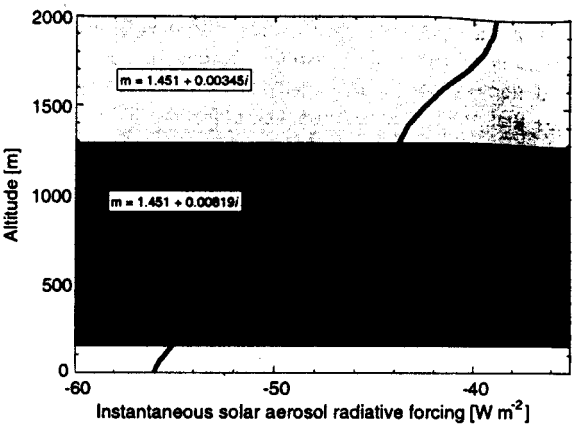

Figure 8. Vertical profile of the instantaneous shortwave aerosol radiative forcing, as calculated by the Fu-Liou radiative transfer model for TARFOX case study 2, July 24, 1996, 1500 GLT for a surface albedo A_S of 4.3% and μ_0 of 0.74. The forcing at the top of the atmosphere is -36.87 W m^{-2}.

Figure 8 shows the vertical profile of the instantaneous shortwave aerosol radiative forcing for this case study. The ocean surface albedo and the cosine of the solar zenith angle at this time and location are 4.3% and 0.74%, respectively. The aerosol radiative forcing at the top of the atmosphere amounts to -37 W m^{-2}, and the forcing at the surface is again of the order of -56 W m^{-2}.

As in the first case study, we can place these results in perspective by calculating the diurnal variations of the shortwave aerosol radiative forcings at the top of the atmosphere (TOA) and at the top of the aerosol layer (TOL). Again, this simulation does not include any time evolution of the aerosol but merely the changes in the solar zenith angle and the surface albedo for this case study as a function of the Genuine Local Time (GLT). Figure 9 shows the distinct noontime minimum of the aerosol radiative forcing and maxima in the midmorning and

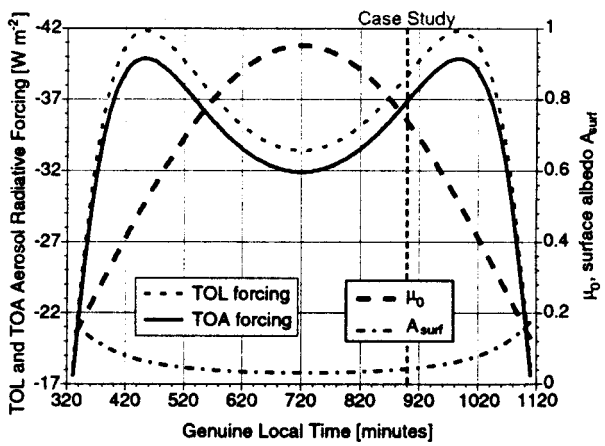

Figure 9. Estimate of the diurnal variation of the instantaneous shortwave aerosol radiative forcing, as calculated by the Fu-Liou radiative transfer model for TARFOX case study 2, July 24, 1996, for the top of the atmosphere (solid line) and the top of the aerosol layer (short-dashed line) by varying only the solar zenith angle and the ocean surface albedo with time. Ocean surface albedo and μ_0 are indicated.

midafternoon. For this case study, however, the absolute difference between the TOA radiative forcing at local noon and at the midafternoon maximum is only of the order of 6 W m^{-2}. This implies that the instantaneous value for the TOA forcing of -37 W m^{-2} in Figure 6 (at 1500 GLT) is very close to the afternoon maximum of -39.5 W m^{-2}.

4. Error Propagation in Radiative Transfer Modeling Results

The radiative forcing calculations presented here are the result of simulations using the Fu-Liou radiative transfer model. Therefore an analysis of the error propagation from the model input parameters into the radiative flux results must be performed by means of a sensitivity study, as opposed to an error estimate based on analytical expressions. For legibility, let F be the aerosol-induced radiative forcing at the top of the atmosphere and let us assume that F is a function of the aerosol optical depth τ, the single-scattering albedo ω, the aerosol asymmetry parameter g, the surface albedo A_S, and the cosine of the solar zenith angle $\mu_0 = \cos\theta_0$; hence $F = F(\tau, \omega, g, A_S, \mu_0)$. Assuming that the error in the forcing is proportional to the errors in the input parameters, we can write the absolute error in the forcing ΔF as follows [cf. *Bevington*, 1969]:

$$\Delta F \equiv \Delta\tau\left(\frac{\partial F}{\partial \tau}\right) + \Delta\omega\left(\frac{\partial F}{\partial \omega}\right) + \Delta g\left(\frac{\partial F}{\partial g}\right) + \Delta A_S\left(\frac{\partial F}{\partial A_S}\right) + \Delta\mu_o\left(\frac{\partial F}{\partial \mu_o}\right). \quad (4)$$

The terms on the right-hand side of (4) were estimated by calculating the model response to realistic errors in the input parameters. Table 2 summarizes the results from this type of sensitivity analysis for the two TARFOX case studies presented in this paper. Errors in the aerosol optical depth were estimated to be of the order of 10%; the single-scattering albedo was also varied by 10%, and the asymmetry parameter was varied by only 5%, based on the fact that it usually exhibited less variability than the other two aerosol parameters. The surface albedo A_S was changed by 20% from its central value, while the solar zenith angle was varied by 1°. We believe that the above uncertainties represent the maximum range of possible errors, rather than a one standard deviation from the mean values. The 10% error in the single-scattering albedo may appear large but is well within the range of values determined during the TARFOX experiment [*Hegg et al.*, 1997; *Hartley et al.*, this issue]. However, by using relatively large values for the uncertainties in the aerosol single-scattering properties, we intended to quantify the maximum error in our aerosol radiative forcing results.

Table 2. Analysis of the Sensitivity of the Fu-Liou Radiative Transfer Model for the Radiative Forcing at the Top of the Atmosphere F for the two TARFOX Case Studies Discussed in This Paper

	TOA Forcing (W m^{-2}) and Deviation From Baseline Forcing (%) TARFOX	
	July 17, 1996	July 24, 1996
Baseline forcing, W m^{-2}	-36 (NA)	-37 (NA)
τ + 10%	-39 (+9.6%)	-40 (+9.3%)
τ - 10%	-32 (-9.9%)	-33 (-9.4%)
ω - 10%	-24 (-33.0%)	-26 (-28.9%)
g + 5%	-30 (-15.5%)	-33 (-10.3%)
g - 5%	-41 (+15.5%)	-41 (+10.2%)
A_S + 20%	-35 (-1.4%)	-36 (-2.4%)
A_S - 20%	-37 (+2.5%)	-38 (+2.5%)
θ_0 + 1°	-36 (+1.1%)	-37 (+1.1%)
θ_0 - 1°	-36 (-1.1%)	-36 (-0.8%)

The sensitivity is given in the form of the calculated TOA forcings (in W m^{-2}) and deviations from the baseline forcing (in %) in response to changes in the input parameters (column 1). Deviations from the baseline forcings are calculated using floating point precision

The results in Table 2 show that the TARFOX radiative forcing estimates are most sensitive to the 10% change in the aerosol single-scattering albedo and somewhat less sensitive to changes in the aerosol optical depth and the asymmetry parameter. The change in the single-scattering albedo reduces the magnitude of the negative radiative forcings by about 30%, while the variations in the aerosol optical depth and asymmetry factor result in ~10% changes in the TOA forcing. Thus the changes in the aerosol parameters have the largest impact on the aerosol radiative forcing, while moderate errors in the estimates of the surface albedo and the solar zenith angle have negligible effects on the accuracy of the radiative forcing results, likely because of the large magnitude of the TOA radiative forcing. The results in Table 2 further suggest that the sensitivity of the radiative forcing to changes in all of the input parameters is fairly linear in the range of parameters considered here.

Table 2 shows that equation (4) is not likely to produce an accurate value for the absolute error in the aerosol radiative forcing at TOA for the following reason. Equation (4) assumes that the errors in the variables are small and, more importantly, that they are independent of each other. However, errors in the aerosol parameters (extinction, single-scattering parameter, and asymmetry parameter) are necessarily a consequence of errors in the fundamental aerosol properties (i.e., the aerosol size distribution and/or complex index of refraction). For example, an increase in the imaginary part of the aerosol index of refraction will increase the aerosol optical depth and, at the same time, decrease the single-scattering albedo. According to Table 2 these two circumstances (increased aerosol optical depth and decreased single-scattering albedo) have opposite effects on the TOA aerosol radiative forcing for both of the TARFOX case studies presented here.

From the above considerations we can conclude that the error in TOA aerosol radiative forcing can be assessed more realistically by carrying out a sensitivity analysis with respect to the complex aerosol refractive indices and the aerosol particle size distributions. In the technique for estimating the refractive index developed by *Redemann et al.* [this issue] the *in situ* particle size distributions were adjusted to yield closure with the sunphotometer-derived aerosol optical depths. This adjustment was performed because the aerosol refractive indices retrieved from the lidar backscatter profiles and the original particle size distributions did not reproduce the independent sunphotometer aerosol optical depths. Hence the study by *Redemann et al.* [this issue] produced two sets of particle size distribution and aerosol refractive index data. The first one reproduces the lidar-derived aerosol backscatter on the basis of the original particle size distributions but does not yield closure with the

Table 3. Calculations of the TARFOX TOA Aerosol Radiative Forcing on the Basis of the Different Sets of Aerosol Size Distributions and Corresponding Retrieved Aerosol Refractive Indices

	Retrieved Refractive Indices and TOA Forcing (W m^{-2}) TARFOX			
	Refractive indices for July 17, 1996	TOA forcing for July 17, 1996	Refractive indices for July 24, 1996	TOA forcing for July 24, 1996
Original size distributions	$m_1 = 1.499 - 0.00009i$ $m_2 = 1.547 - 0.00278i$ $m_3 = 1.499 - 0.00180i$	-31	$m_1 = 1.547 - 0.00278i$ $m_2 = 1.451 - 0.00819i$	-34
Adjusted size distributions	$m_1 = 1.330 - 0.00117i$ $m_2 = 1.378 - 0.00428i$ $m_3 = 1.451 - 0.00224i$	-36	$m_1 = 1.451 - 0.00345i$ $m_2 = 1.451 - 0.00819i$	-37

sunphotometer-derived aerosol optical depths. The second one yields aerosol refractive indices and adjusted particle size distributions, which are in accord with both the lidar-derived aerosol backscatter and the sunphotometer-derived aerosol optical depths (for details on the required adjustment to the particle size distribution measurements, see *Redemann et al.* [this issue]). Surprisingly, the aerosol radiative forcings calculated on the basis of the original aerosol size distributions and the corresponding retrieved aerosol refractive indices did not vary by more than 15% from the values calculated based on the adjusted size distributions and their corresponding retrieved refractive indices (compare Table 3).

The reason for this lack of sensitivity in the aerosol radiative forcing calculations is that the retrieved aerosol refractive indices are based on a certain set of particle size distributions and that, in some sense, the retrieved refractive indices compensate for errors in the *in situ* particle size distributions in order to reproduce the lidar backscatter measurements. This sensitivity study shows that a TOA aerosol radiative forcing estimate can be accurate, provided the set of particle size distributions and refractive index data properly represent aerosol backscattering. This result is not surprising, considering that in simplified analytical expressions the aerosol radiative forcing is proportional to the hemispheric aerosol upscattering (i.e., the scattering integrated over the backward hemisphere [e.g., *Russell et al.*, 1997]).

Finally, to assess the uncertainties in the radiative forcing calculations caused by independent errors in the retrieved aerosol refractive indices, Table 4 shows the sensitivity of the TARFOX radiative forcing results to a 20% error in the imaginary part and a 5% error in the real part of the retrieved aerosol refractive indices (without any adjustments to the *in situ* particle size distributions). These errors were selected based on a sensitivity study for the TARFOX refractive index retrieval technique [cf., *Redemann et al.*, this issue], which approximately yielded the above errors in aerosol refractive indices as a consequence of 30%-random errors in the input lidar backscatter data.

Summarizing Table 4, the TARFOX TOA radiative forcings show a strong sensitivity to errors in the real part of the aerosol refractive indices (on the order of 30% to a 5% change in m_r) and are less sensitive to errors in the imaginary part. Undoubtedly, this is caused by the small absolute values of the imaginary parts of the retrieved refractive indices, for which a 20% change does not produce major changes in the derived aerosol properties (extinction, single-scattering albedo, and asymmetry parameter). However, the sensitivity of the aerosol radiative forcing estimates to the imaginary refractive indices is likely greater for aerosols with imaginary refractive indices above 0.01. In conclusion, the TARFOX TOA aerosol radiative forcing estimates are likely to have maximum uncertainties of the order of ±12 W m^{-2} corresponding to relative errors of ±30%.

5. Discussion

The shortwave aerosol radiative forcing calculations for the two TARFOX case studies discussed here yield very comparable top of the atmosphere forcings of -36 and -37 W m^{-2}. This similarity can be attributed to the comparable aerosol optical depths for the two cases (about 0.5 in the midvisible), and the fact that the case studies took place at about the same time of the day. The aerosol-induced flux changes at the surface are about -56 W m^{-2}, implying a strong cooling effect in the surface layers. These calculations are based on effective aerosol refractive index estimates obtained from a combination of lidar-derived aerosol backscatter, sunphotometer-derived aerosol extinction, and *in situ* particle size distributions [*Redemann et al.*, this issue]. Since a number of investigators [e.g., *Ackerman and Toon*, 1981; *Bohren and Huffman*, 1983] have pointed out that an effective refractive index, as derived from an optical scattering measurement, may lead to erroneous estimates of the aerosol absorption coefficient (and the single-scattering albedo), we intercompared our single-scattering albedo profiles to independent measurements by *Hartley et al.* [this issue]. In general, the data sets agreed within

Table 4. Analysis of the Sensitivity of the Fu-Liou Radiative Transfer Model for the Radiative Forcing at the Top of the Atmosphere F for the two TARFOX Case Studies Discussed in This Paper With Respect to Changes in the Retrieved Aerosol Indices of Refraction

	TARFOX July 17, 1996	TARFOX July 24, 1996
Baseline forcing, W m^{-2}	-36	-37
Forcing (W m^{-2}) with m_r - 5%	-24 (-32.2%)	-27 (-26.8%)
Forcing (W m^{-2}) with m_i + 20%	-34 (-5.1%)	-35 (-5.0%)

The sensitivity is given in the form of the calculated TOA forcings (in W m^{-2}) and deviations from the baseline forcing (in %) in response to the changes in the input parameters (column 1). Deviations from the baseline forcings are calculated using floating point precision.

the measurement uncertainties and showed very good agreement in those parts of the profiles where most of the extinction occurs. Therefore we conclude that our single-scattering albedo estimates are valid and hence appropriate for radiative forcing calculations as carried out here.

Russell et al.[1999b] calculated the aerosol-induced changes in the upward and downward irradiances for several TARFOX flights and showed generally good agreement between their theoretical values and values obtained from pyranometer measurements aboard the U.K. Meteorological Office C-130 aircraft [*Hignett et al.*, 1999]. In particular, they investigated the aerosol radiative effects for a case study on July 17, which took place only three hours before the first case study of this work. The diurnal variation in the aerosol-induced changes in the upward irradiance for July 17 given by *Russell et al.* [1999b] (their Figure 7) is similar to the diurnal forcing calculations given here (see Figure 4), suggesting the validity of their simplified flux calculation method.

It is noteworthy that both TARFOX cases studied here yield only a small difference (approximately 2 W m^{-2}) between the forcing at the top of the aerosol layer (TOL) and the top of the atmosphere (TOA); see Figures 5 and 9. If the forcing at the TOL was caused solely by the aerosol-induced change in the upward irradiance, one would expect that the TOA forcing is simply the product of the TOL forcing and the transmission of the overlying atmosphere. Assuming, for example, a TOL forcing of -35 W m^{-2} and a transmission of 0.8, one would derive a TOA forcing of -28 W m^{-2} and hence a difference between the two forcings of the order of 7 W m^{-2}, rather than 2 W m^{-2} obtained from the detailed radiative transfer model calculations. The explanation for this apparent discrepancy lies in the aerosol-induced changes in the downward irradiance at TOL. Table 5 gives the detailed flux results at TOL and TOA for our July 17, 1996, case study .

Table 5 confirms that the TOA aerosol radiative forcing is caused by the aerosol-induced change in the upward irradiance only. However, the TOL aerosol radiative forcing caused by an increase in the upwelling component ($\Delta F\uparrow$) of the net flux by 41.51 W m^{-2} is reduced by a simultaneously increased downwelling irradiance. The change in the downwelling flux at TOL is only 4.3 W m^{-2} but is large enough to reduce the difference between the TOL and the TOA radiative forcings to 1.3 W m^{-2}.

Table 5. Detailed Results of Shortwave Radiative Flux Calculations (in W m^{-2}) at Top of the Aerosol Layer (TOL) and at Top of the Atmosphere (TOA) With the Fu-Liou Radiative Transfer Model for TARFOX Case Study 1, July 17, 1996

	Model Run Results With Aerosols		Model Run Results Without Aerosols		Change in Upward Flux	Radiative Forcing
	$F\downarrow$	$F\uparrow$	$F\downarrow$	$F\uparrow$	$\Delta F\uparrow$	ΔF
TOA	1109.6	118.5	1109.6	82.6	-35.9	-35.9
TOL	1000.6	97.5	996.3	56.0	-41.5	-37.2

6. Conclusions

The finding of an aerosol-induced change in the downwelling component of the net flux at the top of an aerosol layer is an important result which shows that while the dominant factor in the aerosol radiative forcing at a given level in the atmosphere is the change in the upwelling component, the downwelling can also be significant. Thus for the determination of aerosol-induced flux changes in the atmosphere, both the upwelling and the downwelling components of the net flux need to be measured. Importantly, these conclusions can only be drawn from detailed radiative transfer calculations that consider the vertical structure of the aerosol radiative forcing based on vertically resolved information regarding the aerosol optical and microphysical properties (obtained here through synthesis of lidar, sunphotometer, and *in situ* particle size distribution data). The vertical distribution of the aerosol radiative forcing is relevant to climate studies since it affects convection and the formation and lifetime of clouds. An application of the multi-instrument approach, as outlined here, to different aerosol data sets will likely provide a comprehensive picture of the vertical structure of tropospheric aerosol radiative forcing and hence improve our understanding of climate responses to aerosol-induced changes in Earth's radiation balance.

Acknowledgments. TARFOX is a contribution to the International Global Atmospheric Chemistry (IGAC) core project of the International Geosphere-Biosphere Programme (IGBP). The authors would like to thank D. McIntosh (Symtech, Corp.) for support during the preparation of this manuscript. This work was funded under NSF grants ATM-96-18425 and ATM-94-12082. Support through NASA radiation science program, codes 622-44-10-10 and 622-44-75-10, and NASA grant NAGS-7675 is also gratefully acknowledged.

References

Ackerman, T.P., and O.B. Toon, Absorption of visible radiation in atmosphere containing mixtures of absorbing and nonabsorbing particles, *Appl. Opt., 20,* 3661-3668, 1981.

Bevington, P.R., Data reduction and error analysis for the physical sciences, McGraw-Hill, New York, 1969.

Bohren, C. F., and D.R. Huffman, *Absorption and Scattering of Light by Small Particles*, John Wiley, New York, 1983.

Briegleb, B.P., and V. Ramanathan, Spectral and diurnal variations in clear sky planetary albedo, *J. Appl. Meteorol., 25,* 214-226, 1982.

Browell E.V., et al., LASE validation experiment, in *Advances in Atmospheric Remote Sensing With Lidar,* pp. 289-295, Springer-Verlag, New York, 1996.

Ferrare, R.A., et al., Comparison of aerosol optical properties and water vapor among ground and airborne lidars and sunphotometers during TARFOX, *J. Geophys. Res.*, this issue.

Fu, Q., and K.N. Liou, On the correlated k-distribution method for radiative transfer in nonhomogeneous atmospheres, *J. Atmos. Sci., 49,* 2139-2156, 1992.

Fu, Q., and K.N. Liou, Parameterization of the radiative properties of cirrus clouds, *J. Atmos. Sci., 50,* 2008-2025, 1993.

Glew, M.D., P. Hignett, and J.P. Taylor, Aircraft measurements of sea surface albedo, *J. Geophys. Res.*, in press, 1998.

Hansen, J., M. Sato, and R. Ruedy, Long-term changes of the diurnal temperature cycle: Implications about mechanisms of global climate change, *Atmos. Res., 37,* 175-209, 1995.

Hansen, J., M. Sato, and R. Ruedy, Radiative forcing and climate response, *J. Geophys. Res., 102,* 6831-6864, 1997.

Hartley, W.S., P.V. Hobbs, J.L. Ross, and P.B. Russell, Properties of aerosols aloft relevant to direct radiative forcing off the mid-Atlantic coast of the United States, *J. Geophys. Res.*, this issue.

Haywood, J.M., and V. Ramaswamy, Global sensitivity studies of the direct radiative forcing due to anthropogenic sulfate and black carbon aerosols, *J. Geophys. Res., 103,* 6043-6058, 1998.

Hegg, D.A., J.M. Livingston, P.V. Hobbs, T. Novakov, and P.B. Russell, Chemical apportionment of aerosol column optical depth off the mid-Atlantic coast of the United States, *J. Geophys. Res.*, 1997.

Hobbs, P.V., An overview of the University of Washington airborne

measurements and results from the Tropospheric Aerosol Radiative Forcing Observational Experiment (TARFOX), *J. Geophys. Res.*, *104*, 2233-2238, 1999.

Intergovernmental Panel on Climate Change (IPCC), *Report of the IPCC (Intergovernmental Panel on Climate Change 1994) to the First Session of the Conference of the Parties to the UN Framework Convention on Climate Change*, chap. 3, Cambridge Univ. Press, New York, 1995.

Lowenthal, D.H., C.F. Rogers, P. Saxena, J.G. Watson, and J.C. Chow, Sensitivity of estimated light extinction coefficients to model assumptions and measurement errors, *Atmos. Environ.*, *29*, 751-766, 1995.

Novakov, T., D.A. Hegg, and P.V. Hobbs, Airborne measurements of carbonaceous aerosols on the east coast of the United States, *J. Geophys. Res.*, *102*, 30,023-30,030, 1997.

Redemann, J., et al., Retrieving the vertical structure of the effective aerosol complex index of refraction from a combination of aerosol *in situ* and remote sensing measurements during TARFOX, *J. Geophys. Res.*, this issue.

Russell, P.B., S. Kinne, and R. Bergstrom, Aerosol climate effects: Local radiative forcing and column closure experiments, *J. Geophys. Res.*, *102*, 9397-9407, 1997.

Russell, P.B., P.V. Hobbs, and L.L. Stowe, Aerosol properties and radiative effects in the United States east coast haze plume: An overview of the Tropospheric Aerosol Radiative Forcing Experiment (TARFOX), *J. Geophys. Res.*, *104*, 2213-2222, 1999a.

Russell P.B., J.M. Livingston, P. Hignett, S. Kinne, J. Wong, A. Chien, P. Durkee, and P.V. Hobbs, Aerosol-induced radiative flux change off the United States mid-Atlantic coast: Comparison of values calculated from sunphotometer and *in situ* data with those measured by airborne pyranometer, *J. Geophys. Res.*, *104*, 2289-2307, 1999b.

Taylor, J.P., J.M. Edwards, M.D. Glew, P. Hignett, and A. Slingo, Studies with a flexible new radiation code, II. Comparisons with aircraft short-wave observations, *Q.J.R. Meteorol. Soc.*, *122*, 839-861, 1996.

Tett, S.F.B., J.F.B. Mitchell, D.E. Parker, and M.R. Allen, Human influence on the atmospheric vertical temperature structure: Detection and observations, *Science*, *274*, 1170-1173, 1996.

J. Redemann and R.W. Bergstrom, Bay Area Environmental Research Institute, San Francisco, CA 94122. (jredemann@mail.arc.nasa.gov)

R.P. Turco and K.N. Liou, Department of Atmospheric Sciences, UCLA, Los Angeles, CA 90095.

P.V. Hobbs and W.S. Hartley, Department of Atmospheric Sciences, University of Washington, Seattle, WA 98195-1640.

E.V. Browell, NASA Langley Research Center, Hampton, VA 23681-0001.

P.B. Russell, NASA Ames Research Center, MS 245-5, Moffett Field, CA 94035-1000.

(Received June 25, 1999; revised October 1, 1999;
accepted October 6, 1999.)